Transition strengths in odd-odd ^{80}Rb

M. A. Cardona,[1,2] G. García Bermúdez,[1,2,3] R. A. Kaye,[4] G. Z. Solomon,[4] and S. L. Tabor[4]
[1]*Departamento de Física, Comisión Nacional de Energía Atómica, 1429 Buenos Aires, Argentina*
[2]*Escuela de Ciencia y Tecnología, Universidad de San Martín, Argentina*
[3]*CONICET, 1033 Buenos Aires, Argentina*
[4]*Department of Physics, Florida State University, Tallahassee, Florida 32306*
(Received 28 June 1999; published 13 March 2000)

Lifetimes of levels in ^{80}Rb have been measured using the Doppler shift attenuation method. The high-spin states have been populated through the ^{55}Mn(^{28}Si,$2pn$) reaction at 90 MeV. Collective enhancement was observed in the $B(E2)$ values of the two most strongly populated bands, while the $B(M1)$ values of the yrast band exhibit a large alternating pattern. Transition quadrupole moments were deduced from $E2$ transition strengths and compared with those predicted by Woods-Saxon cranking calculations.

PACS number(s): 21.10.Tg, 27.50.+e, 29.30.Kv

I. INTRODUCTION

One interesting feature of nuclei in the mass $A \approx 80$ region is the strong shape variation as a function of both particle number and spin. In particular, different deformations have been observed in the same nucleus, leading to the concept of shape coexistence. The microscopic structure of these nuclei is primarily dominated by the $1g_{9/2}$, $2p_{1/2}$, $1f_{5/2}$, and $2p_{3/2}$ orbitals for both protons and neutrons. These orbitals show considerable single-particle energy gaps for large quadrupole deformations.

In the odd-odd nuclei of this mass region the nuclear structure shows a complex low-lying level scheme up to $\approx$0.5 MeV, and above this energy the decay scheme presents a more regular pattern of rotational bands. In particular, this behavior has been found in ^{80}Rb which displays an extremely complicated low spin structure [1,2]. At higher energy, a regular increase in level energy and the presence of crossover transitions are clear signatures of collective bands [2–5].

Another feature observed in the structure of $A \approx 80$ odd-odd nuclei is the phenomenon of signature inversion. At spins above about $10\hbar$ the odd and even spin states (with signatures $\alpha=1$ and 0) in the positive-parity band of $\pi g_{9/2} \otimes \nu g_{9/2}$ parentage are not evenly spaced. Instead the odd spin states lie relatively lower in energy, resulting in significant signature splitting. However, as the band is followed to lower spins, the signature splitting reverses, with the even spin states lying relatively lower in energy. Several mechanisms have been proposed for this inversion in signature splitting, but the theoretical calculations have not been conclusive.

In order to study the deformation of the different rotational structures in ^{80}Rb and to determine the electromagnetic transition strengths in the region where signature inversion takes place, lifetimes were measured using the Doppler-shift attenuation method (DSAM). The determination of lifetimes allows the calculation of transition strengths, transition quadrupole moments and quadrupole deformations, which provide information about the degree of collectivity and could help elucidate the mechanism of the signature inversion phenomenon.

II. EXPERIMENTAL PROCEDURE

The fusion-evaporation reaction ^{55}Mn(^{28}Si,$2pn$) at 90 MeV was used to study high-spin states in ^{80}Rb. The beam was provided by the Florida State University Tandem-LINAC facility. A thick target of natural Mn foil of thickness 18 mg/cm^2 was used to stop the recoiling nuclei. A γ-γ coincidence experiment was performed using the Pitt-FSU detector array [6], which consisted in this experiment of 10 high-purity Compton-suppressed Ge detectors placed at a distance of 15 cm from the target. Four Ge detectors were placed at 90° relative to the beam axis, four were located at 145° and the remaining two were placed at 35°. A total of 1.5×10^8 prompt γ-γ coincidence events were recorded.

The data were sorted into different matrices. Two symmetrized matrices, one of them using the coincidences between any pair of detectors and the other using only those at 90°, were built. In addition two different square matrices were constructed for lifetime analysis. One of them stored the events in which one γ ray was measured in the 35° detectors and the other one in the 90° detectors. The other array collected γ-γ coincidences between detectors at 145° and 90°. In these latter two arrays, gates were set on ^{80}Rb lines on the axis corresponding to the 90° detectors and were added to improve statistical accuracy for each set of data. These 35° and 145° projected spectra provided the line shapes for the determination of lifetimes using the DSAM.

III. LIFETIME MEASUREMENTS

Lifetimes of 13 levels and upper limits for 4 levels in ^{80}Rb were determined in this work. For reference a partial level scheme of ^{80}Rb showing the two most strongly populated bands, as reported recently in Refs. [2,4,5], is shown in Fig. 1. The excitation energies of the 6^+ and (4^-) states are from Ref. [2] and the transition energies correspond to the values measured in the present experiment. Both bands indicated in Fig. 1 were populated in the reaction used here. Sum

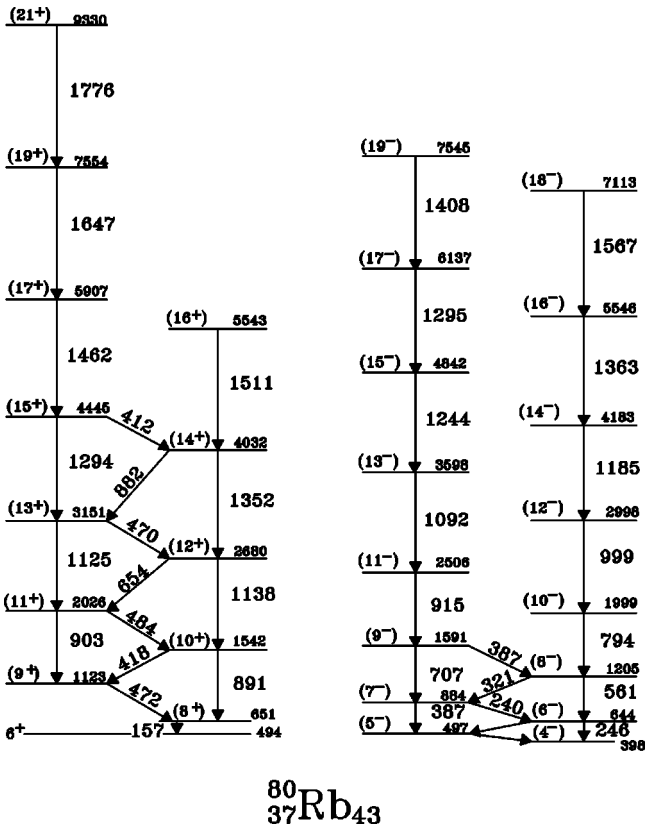

$^{80}_{37}Rb_{43}$

FIG. 1. Partial level scheme of ^{80}Rb [2,4,5].

coincidence spectra produced by gating on transitions belonging to the positive- and negative-parity bands in the symmetrized 90° matrix are shown in Figs. 2(a) and 2(b), respectively.

The deduced lifetimes are sensitive to a correct evaluation of the intensities of all feeding transitions. To avoid contaminations, the γ-ray intensities were determined from gated

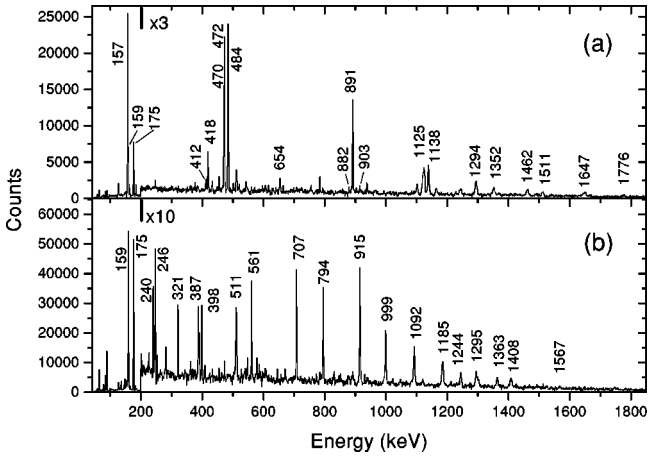

FIG. 2. Sum of spectra in coincidence with transitions in the positive- (a) and negative-parity (b) bands of ^{80}Rb displayed at 90°. Transitions in these bands are labeled with their energy in keV. Also indicated in the spectra are the strong lines of 159 and 175 keV belonging to the low-energy structure of ^{80}Rb and in part (b) the 398 keV line which depopulates the negative-parity band.

spectra at 90° and were corrected for angular distribution effects. This correction was performed assuming $A_2 = -0.38$ and $A_2 = +0.38$ for $\Delta I = 1$ and $\Delta I = 2$ transitions, respectively, with higher order coefficients set to zero. Table I summarizes the γ-ray intensities of interest in the present work for the determination of lifetimes and branching ratios.

The line shapes in the 35° and 145° coincidence spectra were analyzed using a computer code [7] which simulates the slowing down process of the recoiling nuclei. In the calculation the thick target is divided into a large number of layers. The nuclear and electronic stopping powers were extracted from Ref. [8]. The production of residual nuclei in each target layer was weighted by the cross section at the average beam energy in that layer which was calculated using the statistical model code PACE2 [9]. The distribution of recoil velocities due to particle evaporation and beam deceleration in the target, corrections from direct and cascade feeding, as well as the finite solid angle subtended by the γ-ray detectors were taken into account in the analysis.

The lifetime analysis started with the highest-lying observed transition in a given band for which statistics provided an adequate line shape and then proceeded down the cascade. For the highest analyzed level an effective lifetime was estimated, which contains the contributions of the lifetime of the level and the delays due to side and cascade feeding. This effective value gives an upper limit for the lifetime of the level. The side-feeding times were adopted following a method used in several investigations in this mass region. The method is based on the assignment of a short side-feeding time to the highest measurable state with an increase of about 0.03 ps per MeV of deexcitation energy for levels above an energy of approximately 2.5 MeV [7,10]. In the present work we adopted a side-feeding time of 0.05 ps for the (19^+) state at 7554 keV, with all the other side-feeding times for the levels above 2.5 MeV of excitation energy, based on this value.

For some transitions, especially the strong ones, coincidence spectra gated on lines in the 90° detectors and lying above the level of interest were analyzed. This procedure has the benefit that the line shape is not affected by the side feeding to the relevant level. In turn the general decrease in intensity of higher transitions in the cascade reduces the range of its applicability. When it was possible, both spectra gated above and below the transition of interest were analyzed, providing a way to measure the side-feeding time. The uncertainty of the lifetime values was evaluated by finding the values of τ above and below the best fit value which increased the goodness of fit χ^2 per degree of freedom (χ^2_ν) by one unit.

Let us now discuss in more detail the lifetimes measured in the positive-parity band. Effective lifetimes for the (21^+) and (16^+) states were obtained by analyzing the line shapes of the 1776 and 1511 keV transitions, respectively. The lifetimes of the (19^+), (17^+), and (15^+) states were determined by analyzing the line shapes of the 1647, 1462, and 1294 keV transitions, respectively. For this study both the spectra at 35° and 145° gated with transitions from below were analyzed [Figs. 3(a)–3(e) and 3(g)]. The line shape of the 1352

TABLE I. Relative γ-ray intensities used to evaluate lifetimes and branching ratios in the present work.

E_γ (keV)	$I_i^\pi \rightarrow I_f^\pi$	I_γ	E_γ (keV)	$I_i^\pi \rightarrow I_f^\pi$	I_γ
891	$(10^+)\rightarrow(8^+)$	100(3)	794	$(10^-)\rightarrow(8^-)$	48(2)
418	$(10^+)\rightarrow(9^+)$	13(1)	915	$(11^-)\rightarrow(9^-)$	40(2)
903	$(11^+)\rightarrow(9^+)$	21(1)	999	$(12^-)\rightarrow(10^-)$	33(1)
484	$(11^+)\rightarrow(10^+)$	48(2)	1092	$(13^-)\rightarrow(11^-)$	27(1)
1138	$(12^+)\rightarrow(10^+)$	51(3)	1185	$(14^-)\rightarrow(12^-)$	21(1)
654	$(12^+)\rightarrow(11^+)$	4(1)	1244	$(15^-)\rightarrow(13^-)$	11(1)
1125	$(13^+)\rightarrow(11^+)$	28(2)	1363	$(16^-)\rightarrow(14^-)$	8(1)
470	$(13^+)\rightarrow(12^+)$	12(1)	1295	$(17^-)\rightarrow(15^-)$	9(1)
1352	$(14^+)\rightarrow(12^+)$	21(2)	1567	$(18^-)\rightarrow(16^-)$	2(1)
882	$(14^+)\rightarrow(13^+)$	2(1)	1408	$(19^-)\rightarrow(17^-)$	7(1)
1294	$(15^+)\rightarrow(13^+)$	27(2)			
412	$(15^+)\rightarrow(14^+)$	4(1)			
1511	$(16^+)\rightarrow(14^+)$	12(1)			
1462	$(17^+)\rightarrow(15^+)$	19(1)			
1647	$(19^+)\rightarrow(17^+)$	15(1)			
1776	$(21^+)\rightarrow(19^+)$	9(1)			

keV line at 35° was fitted to establish the lifetime of the (14^+) state [Fig. 3(f)].

The line shape of the 1138 keV transition was obtained from a spectrum gated by the 1352 keV line to reduce interference from the 1125 keV transition [Fig. 4(a)]. A similar difficulty arose in the analysis of the 470 keV line shape with energy close to the 472 keV γ ray. The spectrum gated by the 891 keV transition, which is in coincidence with the 470 keV but not with the 472 keV, improved the measurement [Fig. 3(h)].

The lifetime of the (11^+) state was determined by fitting the line shapes of both the 484 and 903 keV transitions. The side-feeding time of the (11^+) level was directly determined from a comparison of the 484 keV DSA line shapes taken in coincidence with transitions above (1125 keV) [Fig. 4(c)] and below (891 keV) [Fig. 4(e)] this state. The shape of the 484 keV line gated by the 1125 keV yields a level lifetime $\tau_{(11^+)}=0.43(10)$ ps. With this lifetime as a fixed parameter, the fit of the 484 keV line shape in coincidence with the 891 keV yields a side-feeding time to the (11^+) state of $\tau_{sf}=1.0(3)$ ps. This side-feeding time was used in the analysis of the shape of the 903 keV line in coincidence with the 472 keV transition below it [Fig. 4(b)].

The lifetime of the (10^+) state is at the limit of the DSA method; however, Doppler tails in the line shapes are still clearly visible in the detectors at both forward and backward angles in coincidence with the 484 keV line which feeds the (10^+) state [Figs. 4(d) and 4(f)].

In turn, effective lifetimes were established in the negative-parity band for the (16^-) and (15^-) states. The lifetimes of the (14^-), (13^-), and (12^-) states were determined by fitting the line shapes of the 1185, 1092, and 999 keV transitions, respectively. The experimental and fitted line shapes at 35° and 145° are shown in Figs. 5(a)–5(e) and 5(g). Coincidence spectra for the 915 and 794 keV transitions gated by transitions above them are shown in Figs. 5(f) and 5(h), respectively.

The measured lifetimes were obtained from the analysis of the 35° and 145° spectra. Table II summarizes the results and, in column 6, reports the adopted lifetime values.

IV. DISCUSSION

Lifetime measurements are an important tool for the study of the rich variety of different phenomena observed in the $A\approx 80$ mass region. For instance, measurements of transition strengths determine the degree of deformation along a rotational band and might shed some light on signature inversion phenomena.

Transition strengths, $B(M1)$ and $B(E2)$, were determined using the adopted lifetimes, and are listed in Table II. The branching ratios used in the calculation of these quantities were obtained using the γ-ray intensities given in Table I. The magnetic dipole transition strengths $B(M1)$ were evaluated assuming a quadrupole-dipole mixing ratio of $\delta=0$ since $B(M1)$ values are rather insensitive to δ as long as it is small.

The positive-parity band, which corresponds to the yrast structure, has been interpreted in terms of the $\pi g_{9/2}\otimes \nu g_{9/2}$ configuration [2,4,5]. This band shows similarities with bands observed in several neighboring odd-odd nuclei, in particular with respect to large signature splitting and the signature inversion phenomenon. This latter effect involves a reversal in the phase of the alternate odd-even staggering at a certain angular momentum, which for ^{80}Rb is approximately $11\hbar$, as is shown in Fig. 6(a).

Signature inversions in odd-odd nuclei have been found systematically in regions of mass number $A\simeq 80$, 130, and 160 and several explanations have been proposed to describe this phenomenon. Bengtsson *et al.* [11] explained it by the effect of γ deformation in a cranked shell model calculation. Hamamoto [12] using the particle-plus-rotor model suggested that γ deformation may not be so important. The work of Jain *et al.* [13] within the framework of the axially symmetric rotor plus two particles model suggests the mecha-

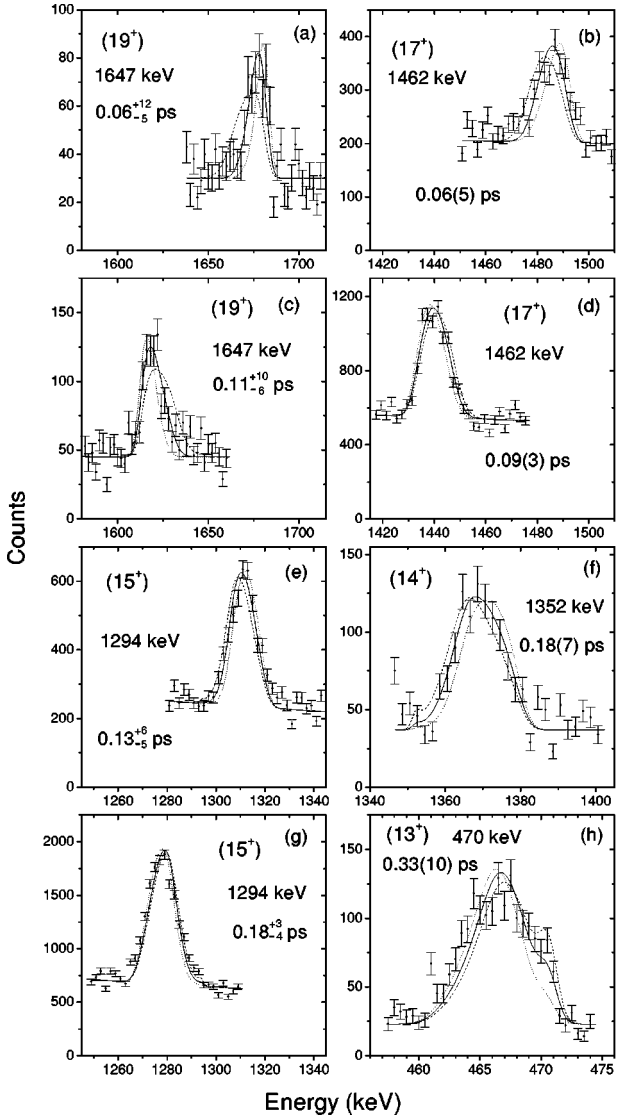

FIG. 3. Doppler-shifted line shapes of the 1647, 1462, 1294, 1352, and 470 keV transitions in the positive-parity band. Spectra shown in (a), (b), (e), and (f) are at 35°, and those shown in (c), (d), (g), and (h) are at 145°. The solid lines indicate the best DSAM fit, while the broken lines correspond to simulations for the indicated error limits which correspond to $\chi^2_{\nu,\min}+1$ fits.

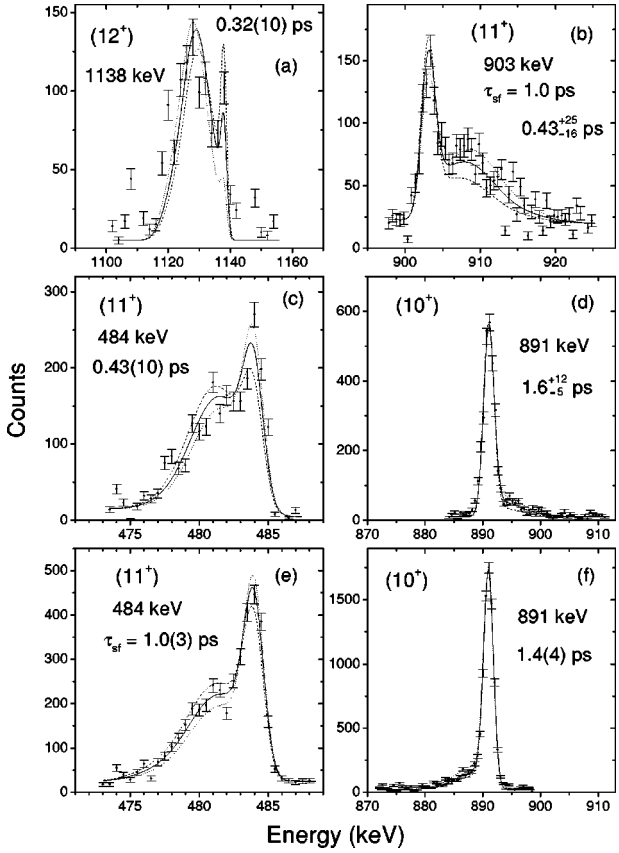

FIG. 4. Doppler-shifted line shapes of the 1138, 903, 484, and 891 keV transitions of the positive-parity band observed at 35° [(b) and (d)] and at 145° [(a), (c), (e), and (f)]. The best fit (solid line) and the $\chi^2_{\nu,\min}+1$ fits (broken lines) are also shown.

nism of Coriolis mixing between a large number of bands and Hara *et al.* [14] proposed the crossing of decoupled bands to describe it. In addition, other studies have analyzed the effect of including the proton-neutron interaction between the odd nucleons (Matsuzaki [15] and Tajima [16]) and the effect of different dynamical symmetries in the interacting boson model (Yoshida *et al.* [17]).

In particular two of the latter calculations predict a signature inversion in the energy splitting as well as in the $B(M1)$ transition strengths. The study of Hamamoto [12] using the particle-plus-rotor model reproduces the inversion in the energy splitting of odd-odd ^{156}Tb rather well. It also reports a perturbation in the $B(M1)$ values with respect to the normal alternation behavior around the signature inversion angular momentum. On the other hand, Womble *et al.* [18] using the same model obtained a rather good fit to the energies and $B(M1)$ strengths. In this study the calculations predicted no change in the phase of the $B(M1)$ alternations. Furthermore Yoshida *et al.* [17] studied the inversion phenomenon within the framework of the interacting boson model and analyzed the effect of the boson core with different dynamical symmetries. Specifically they found an inversion in energy for the $O(6)$ limit of the dynamical symmetry of the boson core with the addition of the proton and neutron exchange interaction. They also observed some effects in the $B(M1)$ alternations around the signature inversion point. In conclusion, a number of studies have proposed a variety of different mechanisms to account for signature inversion. Some predict a change in the normal $B(M1)$ alternations while others do not. Therefore measurements of the $B(M1)$ transition strengths may help to interpret this phenomenon, which is still not well understood.

The measured $B(M1)$ strengths for the positive-parity band are shown in Fig. 6(b) as a function of the angular momentum. As is apparent from the figure, the $B(M1)$ strengths fluctuate and are larger for transitions depopulating odd spin states compared with those deexciting even spin states. This staggering is preserved along the known spin region and, in particular, does not show any noticeable effects across the signature inversion region around $11\hbar$. Previous studies have reported $B(M1)$ strength measurements

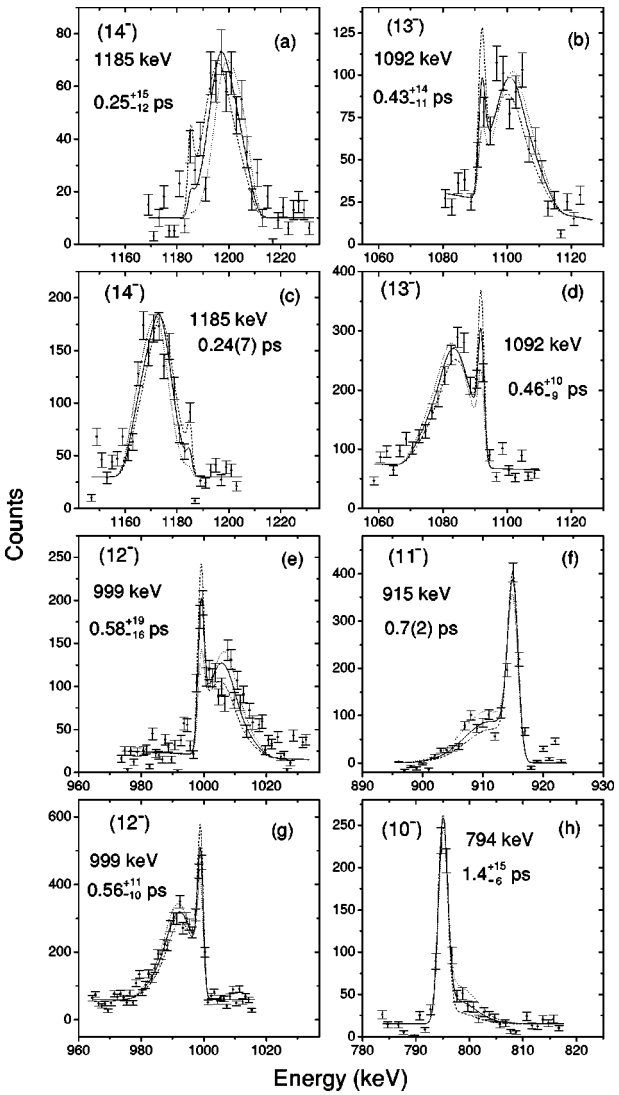

FIG. 5. Doppler-shifted line shapes of the 1185, 1092, 999, 915, and 794 keV transitions belonging to the negative-parity band observed at 35° [(a), (b), (e), and (h)] and at 145° [(c), (d), (f), and (g)]. The best fit (solid line) and the $\chi^2_{\nu,\min}+1$ fits (broken lines) are also shown.

around the signature inversion in the mass 80 region, namely, in ^{74}Br [19,20], ^{78}Rb [21,22], ^{82}Y [23], and ^{84}Y [24]. They arrived at conclusions very similar to those in the present experiment: that the signature inversion does not perturb greatly the $B(M1)$ strength evolution. Thus the experimental results favor mechanisms which predict a normal staggering in the $B(M1)$ values.

Let us analyze the results obtained for the $B(E2)$ strengths. Table II shows that the $E2$ strengths for the positive- and negative-parity bands reveal enhancements by factors of 40 to 90 with respect to the single-particle estimate, with those of the negative-parity band appearing to be higher. These results agree with the characterization, for both cascades of γ rays, as rotational bands with different degrees of collectivity. To examine the evolution of collectivity of the positive-parity bands in neighboring nuclei, we show in Fig. 7 a comparison of the $B(E2)$ strengths for the $(13^+)\rightarrow(11^+)$ transitions for the $\pi g_{9/2}\otimes\nu g_{9/2}$ structures. As can be seen, the $B(E2)$ values for the doubly odd nuclei ^{74}Br [19], ^{76}Br [25], ^{78}Rb [21], ^{80}Rb, ^{82}Y [18], and ^{84}Y [24] show a decrease in collective enhancement, as is expected when the neutron number approaches the shell closure at $N=50$.

From the $B(E2)$ strengths it is possible to calculate the transition quadrupole moments, $|Q_t|$, (Table II) according to the rotational model

$$Q_t^2=\frac{16\pi}{5}\langle IK20|I-2K\rangle^{-2}B(E2,I\rightarrow I-2).$$

An effective value of $K=6$ was used for the positive-parity band. This value of K is consistent with an oblate deformation and the odd proton and neutron lying in the $[413]\frac{7}{2}^+$ and $[422]\frac{5}{2}^+$ orbitals, respectively as reported previously in Ref. [5]. The coupling of both nucleons parallel to each other induces a value of $K=\Omega_p+\Omega_n=6$. The study of Möller *et al.* [26] predicts an oblate deformation for the ground state of ^{80}Rb, and the results of the total Routhian surface (TRS) calculations described below also produce oblate deformed equilibrium shapes over a large range of rotational frequencies. For the negative-parity band we adopted an effective value of $K=3$, as suggested in the work of Tandel *et al.* [5] which assigned an oblate deformation and the configuration $\pi[310]\frac{1}{2}^-\otimes\nu[422]\frac{5}{2}^+$.

Figures 8(a) and 8(b) show the quadrupole moments $|Q_t|$ as a function of rotational frequency for both bands. A small decrease in the $|Q_t|$ values with increasing rotational frequency is apparent. Assuming a constant value along the band, average values of 2.3 and 2.2 e b were obtained for the positive- and negative-parity bands, respectively.

From the transition quadrupole moments, the quadrupole deformations $|\beta_2|$ were inferred using the expression for Q_t corresponding to an axially symmetric nucleus, to first order in β_2,

$$Q_t=\frac{3}{\sqrt{5\pi}}ZeR_0^2\beta_2,$$

with $R_0=1.2A^{1/3}$ fm. The $|\beta_2|$ values range around 0.23–0.37 for both bands (Table II).

Total Routhian surfaces (TRS) were determined from the Woods-Saxon Hartree-Fock-Bogoliubov cranking calculations [27]. They were calculated as a function of the quadrupole deformation of the average nuclear matter distribution β_2^ν, triaxiality parameter γ, and rotational frequency $\hbar\omega$, and were minimized with respect to the hexadecapole deformation β_4 at each $(\beta_2^\nu,\ \gamma)$ point. Figure 9 shows some examples of TRS for different quasiparticle configurations in ^{80}Rb calculated at a given rotational frequency.

For the positive-parity states at low frequencies the calculations predict that the nucleus is γ soft with a quadrupole deformation $\beta_2^\nu\approx0.3$. With increasing frequency, for example at $\hbar\omega=0.492$ MeV, two minima are visible at $\gamma=19°$ and $\gamma=-30°$ [Fig. 9(a)]. The second minimum remains over

TABLE II. Mean lifetimes, electromagnetic transition strengths $B(M1)$, $B(E2)$, transition quadrupole moments $|Q_t|$, and quadrupole deformations $|\beta_2|$ in ^{80}Rb.

$E_{\rm lev}$ (keV)	I^π	E_γ (keV)	τ [a] (ps)	τ [b] (ps)	τ [c] (ps)	$B(M1)$ [d] (W.u.)	$B(E2)$ [e] (W.u.)	$\lvert Q_t\rvert$ (e b)	$\lvert\beta_2\rvert$ [f]
1542	(10^+)	891	1.6^{+12}_{-5}	1.4(4)	1.4(5)		45(16)	2.8(5)	0.37(7)
		418				0.037(14)			
2026	(11^+)	903	0.43^{+25}_{-16}		0.43(12)		46(13)	2.5(4)	0.33(5)
		484		0.43(10)		0.45(13)			
2680	(12^+)	1138		0.32(10)	0.32(10)		61(20)	2.6(4)	0.35(6)
		654				0.025(10)			
3151	(13^+)	1125			0.33(10)		47(15)	2.2(3)	0.29(5)
		470		0.33(10)		0.27(10)			
4032	(14^+)	1352	0.18(7)		0.18(7)		45(18)	2.0(4)	0.27(6)
		882				0.022(10)			
4445	(15^+)	1294	0.13^{+6}_{-5}	0.18^{+3}_{-4}	0.17(4)		56(14)	2.2(3)	0.29(4)
		412				0.34(11)			
5543	(16^+)	1511		<0.23	<0.23		>22	>1.3	>0.18
5907	(17^+)	1462	0.06(5)	0.09(3)	0.08(4)		75(39)	2.4(6)	0.32(8)
7554	(19^+)	1647	0.06^{+12}_{-5}	0.11^{+10}_{-6}	0.08^{+11}_{-5}		41^{+68}_{-24}	1.7^{+11}_{-6}	0.23^{+15}_{-8}
9330	(21^+)	1776		<0.12	<0.12		>19	>1.1	>0.15
1999	(10^-)	794	1.4^{+15}_{-6}		1.4^{+15}_{-6}		90^{+68}_{-47}	2.6(8)	0.35(11)
2506	(11^-)	915		0.7(2)	0.7(2)		89(26)	2.5(4)	0.34(5)
2998	(12^-)	999	0.58^{+19}_{-16}	0.56^{+11}_{-10}	0.57(13)		70(17)	2.2(3)	0.29(4)
3598	(13^-)	1092	0.43^{+14}_{-11}	0.46^{+10}_{-9}	0.45(11)		57(14)	2.0(3)	0.26(3)
4183	(14^-)	1185	0.25^{+15}_{-12}	0.24(7)	0.24(8)		71(24)	2.2(4)	0.29(5)
4842	(15^-)	1244		<0.4	<0.4		>33	>1.5	>0.20
5546	(16^-)	1363		<0.3	<0.3		>28	>1.3	>0.18

[a] Lifetime measured at 35°.
[b] Lifetime measured at 145°.
[c] Adopted lifetime value.
[d] 1 W.u. $= 1.79\mu_N^2$.
[e] 1 W.u. $= 20.5e^2$ fm^4.
[f] Assuming axial symmetry.

the whole range of frequencies measured in the present experiment and evolves towards oblate shapes with increasing frequencies [Fig. 9(b)].

The TRS calculations for the negative-parity states for the π ($p_{1/2}$ or $p_{3/2}$ or $f_{5/2}$) $\otimes \nu g_{9/2}$ configuration predict an oblate equilibrium shape with similar deformation parameters over the whole range of measured frequencies [Figs. 9(c) and 9(d)].

Theoretical transition quadrupole moments were determined from the (β_2^ν, γ) values corresponding to the TRS minima in the range of rotational frequencies for which we have experimental data. The charge quadrupole deformation β_2 derived from $B(E2)$ transition strengths is related to the quadrupole deformation β_2^ν of the nuclear matter distribution derived from Woods-Saxon potential TRS calculations [28–30] by

$$|\beta_2| = 1.1\beta_2^\nu.$$

The relation between β_2 and the quadrupole moment in the case of axial symmetry, $Q_t(\gamma = 0°)$, has been indicated above. In order to take into account a possible triaxiality, we used the high-spin limit for the γ dependence of $|Q_t|$ as given in Refs. [30–32]:

$$|Q_t| = (2/\sqrt{3})Q_t(\gamma = 0°)|\cos(\gamma + 30°)|.$$

The calculated $|Q_t|$ values, obtained from the TRS (β_2^ν, γ) deformations by means of the expressions given above are plotted in Figs. 8(a) and 8(b) as dotted lines for the positive- and negative-parity bands, respectively, showing a good agreement with the experiment.

V. SUMMARY

A γ-γ coincidence experiment with lifetime measurements was performed to study high-spin states of ^{80}Rb populated through the ^{55}Mn(^{28}Si,2pn) reaction at 90 MeV. Lifetimes or upper limits for 17 states have been measured using the DSA method. The $B(M1)$ values of the yrast band display a pronounced staggering which is characteristic of the $\pi g_{9/2} \otimes \nu g_{9/2}$ structure. This staggering is preserved across the angular momentum region in which signature inversion

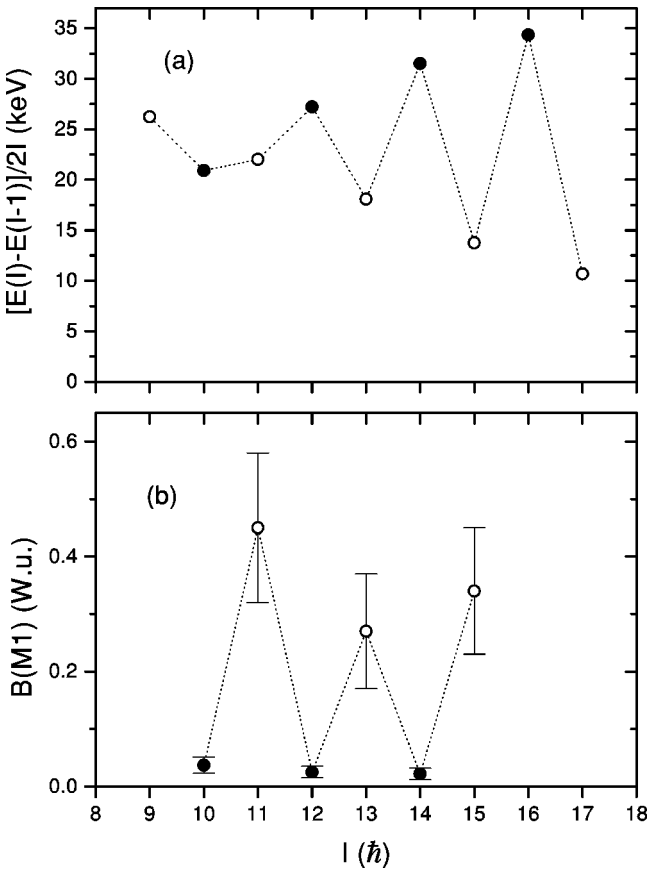

FIG. 6. Signature splitting in the positive-parity band of ^{80}Rb. (a) Normalized energy differences between adjacent levels. (b) $B(M1)$ strengths as a function of the spin of the initial state. Solid and open circles correspond to $\alpha=0$ and $\alpha=1$, respectively.

occurs, in agreement with other recent results [19–23].

Collective enhancement was observed for the $B(E2)$ values. The average transition quadrupole moment of 2.2–2.3 e b for both bands corresponds to an axial quadrupole deformation of $|\beta_2|\approx 0.3$ which is predicted to be near oblate.

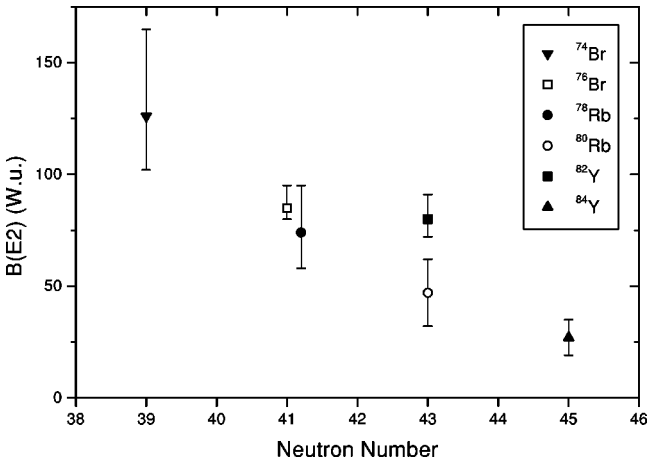

FIG. 7. Comparison of $B(E2)$ ratios of the $(13^+)\rightarrow(11^+)$ transitions in the $\pi g_{9/2}\otimes\nu g_{9/2}$ structures of the odd-odd nuclei ^{74}Br [19], ^{76}Br [25], ^{78}Rb [21], ^{80}Rb (present work), ^{82}Y [18], and ^{84}Y [24].

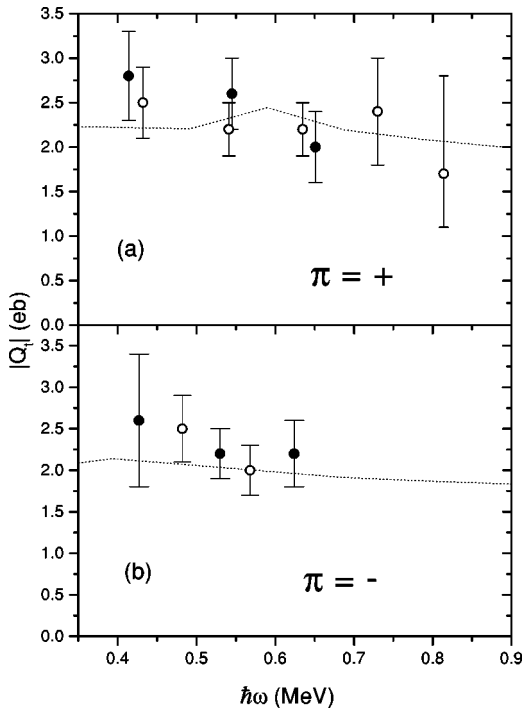

FIG. 8. Transition quadrupole moments $|Q_t|$ plotted vs rotational frequency for (a) positive-parity states and (b) negative-parity states in ^{80}Rb. Solid and open circles correspond to $\alpha=0$ and $\alpha=1$, respectively. The dotted lines represent theoretical values obtained from the TRS calculations as discussed in the text.

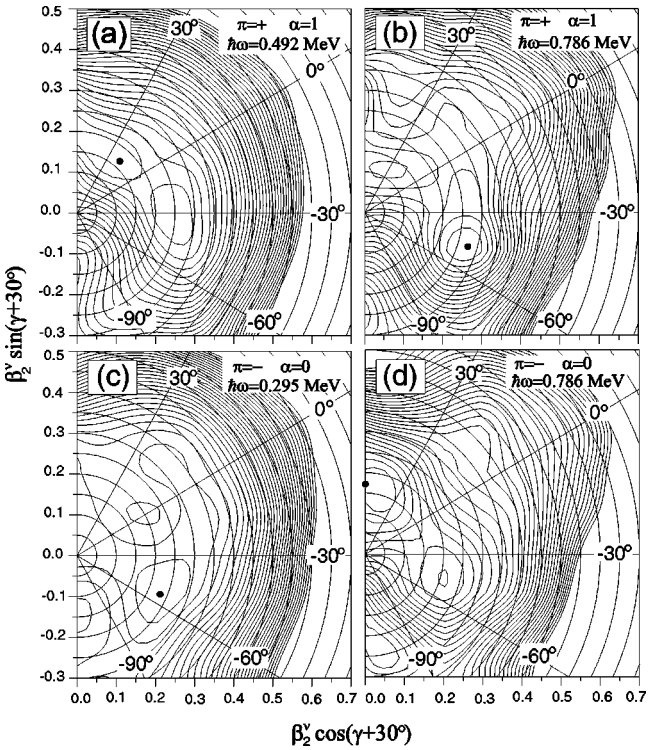

FIG. 9. Total Routhian surfaces in the $(\beta_2^\nu,\ \gamma)$ polar coordinate plane for ^{80}Rb. The band and the rotational frequency are indicated in the inset boxes.

Hartree-Fock-Bogoliubov cranking calculations produce near-oblate deformed equilibrium shapes for both the lowest positive- and negative-parity configurations in ^{80}Rb. Transition quadrupole moments derived from these calculations are in good agreement with those inferred from the lifetime measurements.

ACKNOWLEDGMENTS

This work was supported in part by the NSF-CONICET (Argentina) U.S.-Latin American Cooperative Science Program under Grant No. INT-9314496 and in part by the National Science Foundation under Grant No. PHY-9523974.

[1] M. Behar, A. Filevich, G. García Bermúdez, and M. A. J. Mariscotti, Nucl. Phys. **A287**, 255 (1977).
[2] J. Döring, G. Winter, L. Funke, B. Cederwall, F. Lidén, A. Johnson, A. Atac, J. Nyderg, G. Sletten, and M. Sugawara, Phys. Rev. C **46**, R2127 (1992).
[3] M. A. Cardona, G. García Bermúdez, C. Baktash, M. L. Halbert, D. C. Hensley, N. R. Johnson, I. Y. Lee, F. K. McGowan, M. A. Riley, A. Virtanen, V. Abenante, D. G. Sarantites, T. M. Semkow, and H. C. Griffin, in *Nuclear Structure in the Nineties*, edited by N. R. Johnson (Oak Ridge National Laboratory, Oak Ridge, 1991), Vol. 1, p. 78.
[4] S. K. Tandel, S. B. Patel, R. K. Bhowmik, A. K. Sinha, S. Muralithar, and N. Madhavan, Phys. Rev. C **56**, R2358 (1997).
[5] S. K. Tandel, S. B. Patel, R. K. Bhowmik, A. K. Sinha, S. Muralithar, and N. Madhavan, Nucl. Phys. **A632**, 3 (1998).
[6] S. L. Tabor *et al.*, Nucl. Instrum. Methods Phys. Res. B **79**, 821 (1993).
[7] E. F. Moore, P. D. Cottle, C. J. Gross, D. M. Headly, U. J. Hüttmeier, S. L. Tabor, and W. Nazarewicz, Phys. Rev. C **38**, 696 (1988).
[8] J. F. Ziegler, J. P. Biersack, and U. Littmark, *The Stopping and Range of Ions in Solids* (Pergamon, New York, 1985).
[9] A. Gavron, Phys. Rev. C **21**, 230 (1980).
[10] J. W. Holcomb, J. Döring, T. Glasmacher, G. D. Johns, T. D. Johnson, M. A. Riley, P. C. Womble, and S. L. Tabor, Phys. Rev. C **48**, 1020 (1993).
[11] R. Bengtsson, J. A. Pinston, D. Barneoud, E. Monnand, and F. Schussler, Nucl. Phys. **A389**, 158 (1982).
[12] I. Hamamoto, Phys. Lett. B **235**, 221 (1990).
[13] A. K. Jain and A. Goel, Phys. Lett. B **277**, 233 (1992).
[14] K. Hara and Y. Sun, Z. Phys. A **339**, 15 (1991).
[15] M. Matsuzaki, Phys. Lett. B **269**, 23 (1991).
[16] N. Tajima, Nucl. Phys. **A572**, 365 (1994).
[17] N. Yoshida, H. Sagawa, and J. Otsuka, Nucl. Phys. **A567**, 17 (1994).
[18] P. C. Womble, J. Döring, T. Glasmacher, J. W. Holcomb, G. D. Johns, T. D. Johnson, T. J. Petters, M. A. Riley, V. A. Wood, and S. L. Tabor, Phys. Rev. C **47**, 2546 (1993).
[19] J. W. Holcomb, T. D. Johnson, P. C. Womble, P. D. Cottle, S. L. Tabor, F. E. Durham, and S. G. Buccino, Phys. Rev. C **43**, 470 (1991).
[20] G. García-Bermúdez, M. A. Cardona, A. Filevich, R. V. Ribas, H. Somacal, and L. Szybisz, Phys. Rev. C **59**, 1999 (1999).
[21] R. A. Kaye, J. Döring, J. W. Holcomb, G. D. Johns, T. D. Johnson, M. A. Riley, G. N. Sylvan, P. C. Womble, V. A. Wood, S. L. Tabor, and J. X. Saladin, Phys. Rev. C **54**, 1038 (1996).
[22] R. A. Kaye, L. A. Riley, G. Z. Solomon, S. L. Tabor, and P. Semmes, Phys. Rev. C **58**, 3228 (1998).
[23] G. D. Johns, K. A. Christian, R. A. Kaye, S. L. Tabor, G. García-Bermúdez, M. A. Cardona, A. Filevich, H. Somacal, and L. Szybisz, Phys. Rev. C **53**, 1541 (1996).
[24] S. Chattopadhyay, H. C. Jain, S. D. Paul, J. A. Sheikh, and M. L. Jhingan, Phys. Rev. C **49**, 116 (1994).
[25] S. G. Buccino, F. E. Durham, J. W. Holcomb, T. D. Johnson, P. D. Cottle, and S. L. Tabor, Phys. Rev. C **41**, 2056 (1990).
[26] P. Möller, J. R. Nix, W. D. Myers, and W. J. Swiatecki, At. Data Nucl. Data Tables **59**, 185 (1995).
[27] W. Nazarewicz, J. Dudek, R. Bengtsson, T. Bengtsson, and I. Ragnarsson, Nucl. Phys. **A435**, 397 (1985).
[28] W. Nazarewicz, M. A. Riley, and J. D. Garrett, Nucl. Phys. **A512**, 61 (1990).
[29] J. Dudek, W. Nazarewicz, and P. Olanders, Nucl. Phys. **A420**, 285 (1984).
[30] R. S. Zighelboim, S. G. Buccino, F. E. Durham, J. Döring, P. D. Cottle, J. W. Holcomb, T. D. Johnson, S. L. Tabor, and P. C. Womble, Phys. Rev. C **50**, 716 (1994).
[31] I. Hamamoto and B. R. Mottelson, Phys. Lett. **132B**, 7 (1983).
[32] P. Ring, A. Hayashi, K. Hara, H. Emling, and E. Grosse, Phys. Lett. **110B**, 423 (1982).